

replication at the end of a DNA template. *EMBO J.* **20**, 2914–2922 (2001).

14. McDonald, J. P. *et al.* Novel human and mouse homologs of *Saccharomyces cerevisiae* DNA polymerase η . *Genomics* **60**, 20–30 (1999).
15. Poltoratsky, V. *et al.* Expression of error-prone polymerases in BL2 cells activated for Ig somatic hypermutation. *Proc. Natl Acad. Sci. USA* **98**, 7976–7981 (2001).
16. Zhang, W. *et al.* Clonal instability of V region hypermutation in the Ramos Burkitt's lymphoma cell line. *Int. Immunol.* **13**, 975–984 (2001).
17. Bebenek, K. *et al.* 5'-Deoxyribose phosphate lyase activity of human DNA polymerase ι in vitro. *Science* **291**, 2156–2159 (2001).
18. Petersen-Mahrt, S. K., Harris, R. S. & Neuberger, M. S. AID mutates *E. coli* suggesting a DNA deamination mechanism for antibody diversification. *Nature* **418**, 99–103 (2002).
19. Papavasiliou, F. N. & Schatz, D. G. The activation-induced deaminase functions in a postcleavage step of the somatic hypermutation process. *J. Exp. Med.* **195**, 993–998 (2002).
20. Zeng, X. *et al.* DNA polymerase ϵ is an A-T mutator in somatic hypermutation of immunoglobulin variable genes. *Nature Immunol.* **2**, 537–541 (2001).
21. Rogozin, I. B., Pavlov, Y. I., Bebenek, K., Matsuda, T. & Kunkel, T. A. Somatic mutation hotspots correlate with DNA polymerase ϵ error spectrum. *Nature Immunol.* **2**, 530–536 (2001).
22. Pavlov, Y. I. *et al.* Correlation of somatic hypermutation specificity and A-T base pair substitution errors by DNA polymerase η during copying of a mouse immunoglobulin κ light chain transgene. *Proc. Natl Acad. Sci. USA* **99**, 9954–9959 (2002).
23. Dörner, T., Foster, S. J., Brezinschek, H.-P. & Lipsky, P. E. Analysis of the targeting of the hypermutational machinery and the impact of subsequent selection on the distribution of nucleotides changes in human V(D)J rearrangements. *Immunol. Rev.* **162**, 161–171 (1998).
24. Bachl, J. & Wabl, M. An immunoglobulin mutator that targets G.C base pairs. *Proc. Natl Acad. Sci. USA* **93**, 851–855 (1996).
25. Zan, H. *et al.* The translesion DNA polymerase ζ plays a major role in Ig and bcl-6 somatic hypermutation. *Immunity* **14**, 643–653 (2001).
26. Diaz, M., Verkoczy, L. K., Flajnik, M. F. & Klinman, N. R. Decreased frequency of somatic hypermutation and impaired affinity maturation but intact germinal center formation in mice expressing antisense RNA to DNA polymerase ζ . *J. Immunol.* **167**, 327–335 (2001).
27. Johnson, R. E., Washington, M. T., Haracska, L., Prakash, S. & Prakash, L. Eukaryotic polymerases ι and ζ act sequentially to bypass DNA lesions. *Nature* **406**, 1015–1019 (2000).
28. Mitrucker, H. W., Muller-Fleckenstein, I., Fleckenstein, B. & Fleischer, B. Herpes virus saimiri-transformed human T lymphocytes: normal functional phenotype and preserved T cell receptor signalling. *Int. Immunol.* **5**, 985–990 (1993).
29. de Wind, N., Dekker, M., Berns, A., Radman, M. & te Riele, H. Inactivation of the mouse *Msh2* gene results in mismatch repair deficiency, methylation tolerance, hyperrecombination, and predisposition to cancer. *Cell* **82**, 321–330 (1995).

Supplementary Information accompanies the paper on Nature's website (<http://www.nature.com/nature>).

Acknowledgements We thank B. Fleckenstein for the CB15 cell line; H. Mossafa for the cytogenetic analysis of pol- ι -null clones; R. Woodgate for pol- ι -specific reagents; M. Radman for critically editing the manuscript. This work was supported by the Fondation Princesse Grace de Monaco and the Ligue Nationale Française contre le Cancer (Equipe labellisée). A.F. and S.A. have been supported during part of this work by the Fondation de France (Fondation contre la Leucémie). C.-A.R. and J.-C.W. share senior authorship.

Competing interests statement The authors declare that they have no competing financial interests.

Correspondence and requests for materials should be addressed to J.C.W. (e-mail: weill@necker.fr).

Dual regulation of voltage-gated calcium channels by PtdIns(4,5)P₂

Li Wu*, Claudia S. Bauer*, Xiao-guang Zhen, Cheng Xie & Jian Yang

Department of Biological Sciences, Columbia University, New York, New York 10027, USA

* These authors contributed equally to this work

Voltage-gated calcium channels (VGCCs) conduct calcium into cells after membrane depolarization and are vital for diverse biological events¹. They are regulated by various signalling pathways, which has profound functional consequences^{1,2}. The activity of VGCCs decreases with time in whole-cell and inside-out patch-clamp recordings³. This rundown reflects persistent intrinsic modulation of VGCCs in intact cells. Although several mechanisms have been reported to contribute to rundown of L-

type channels^{3–6}, the mechanism of rundown of other types of VGCC is poorly understood. Here we show that phosphatidylinositol-4,5-bisphosphate (PtdIns(4,5)P₂), an essential regulator of ion channels and transporters^{7–14}, is crucial for maintaining the activity of P/Q- and N-type channels. Activation of membrane receptors that stimulate hydrolysis of PtdIns(4,5)P₂ causes channel inhibition in oocytes and neurons. PtdIns(4,5)P₂ also inhibits P/Q-type channels by altering the voltage dependence of channel activation and making the channels more difficult to open. This inhibition is alleviated by phosphorylation by protein kinase A. The dual actions of PtdIns(4,5)P₂ and the crosstalk between PtdIns(4,5)P₂ and protein kinase A set up a dynamic mechanism through which the activity of VGCCs can be finely tuned by various neurotransmitters, hormones and trophic factors.

P/Q-type Ca²⁺ channels were expressed in *Xenopus* oocytes and macroscopic currents were recorded in giant membrane patches with Ba²⁺ as the external permeant ion. Because depolarization to +100 mV activated nearly all channels (see below), the tail current after such a depolarization (Fig. 1a, $I_{\text{tail}(+100)}$) could be used as a faithful readout of the total number of functional channels and its change with time as a true measure of the time course of rundown. Channel activity stayed constant in the cell-attached mode but waned on excision of inside-out patches (Fig. 1b). The time for $I_{\text{tail}(+100)}$ to decay to 50% of its initial value (T_{50} of rundown) was 5.9 ± 3.2 min ($n = 25$).

To test the effect of PtdIns(4,5)P₂ on rundown, we manipulated the membrane concentration of PtdIns(4,5)P₂ by either applying a brief pulse of PtdIns(4,5)P₂ or sequestering it with a specific antibody (refs 10, 15). A 2-min application of PtdIns(4,5)P₂ immediately after patch excision greatly slowed rundown (Fig. 1b), increasing the T_{50} by 5.4-fold to 32 ± 9.9 min ($n = 6$; Fig. 1c). PtdIns(4,5)P₂ also increased $I_{\text{tail}(+100)}$ when applied after some channels had undergone rundown (Fig. 1d), suggesting that it can reactivate, at least partially, channels that have been rundown already. Conversely, reducing the amount of PtdIns(4,5)P₂ with an antibody against PtdIns(4,5)P₂ accelerated rundown (Fig. 1e). An antibody specific for PtdIns(4)P had no effect at the same concentration. These results suggest that PtdIns(4,5)P₂ stabilizes the activity of P/Q-type channels and its depletion induces rundown.

Notably, P/Q-type channels underwent rundown more slowly when 2 mM Mg-ATP was added to the intracellular solution (Fig. 1c). But this stabilizing effect was not affected by the inclusion of either PKI 5-24, a potent inhibitor of protein kinase A (PKA), or the catalytic subunit of PKA and okadaic acid (an inhibitor of phosphatases 1 and 2A; Fig. 1c), suggesting that other signalling pathways than PKA are involved. A possibility is that Mg-ATP activates membrane-associated lipid kinases to replenish PtdIns(4,5)P₂ (ref. 8). Regardless of the underlying mechanism, sequestering PtdIns(4,5)P₂ with antibodies against PtdIns(4,5)P₂ still markedly accelerated rundown, and this could be partially reversed by subsequent application of PtdIns(4,5)P₂ (Fig. 1f). Together, these results indicate that PtdIns(4,5)P₂ is indispensable for maintaining P/Q-type channel activity in inside-out patches.

Unexpectedly, PtdIns(4,5)P₂ also exerted a voltage-dependent inhibitory effect (Fig. 2a): it inhibited the current elicited by weak depolarizations strongly and the current by intermediate depolarizations moderately, but it had little effect on the outward K⁺ current (flowing through Ca²⁺ channels) evoked by large depolarizations. The activation and peak current voltages were both shifted in the positive direction by 15–20 mV in the presence of PtdIns(4,5)P₂, but the reversal potential was unaffected (Supplementary Information).

The voltage dependence of PtdIns(4,5)P₂ inhibition could be seen more clearly in the tail currents after various depolarizations. In control solution, the tail current after depolarization to +10 mV ($I_{\text{tail}(+10)}$) or +100 mV ($I_{\text{tail}(+100)}$) decayed in parallel after patch

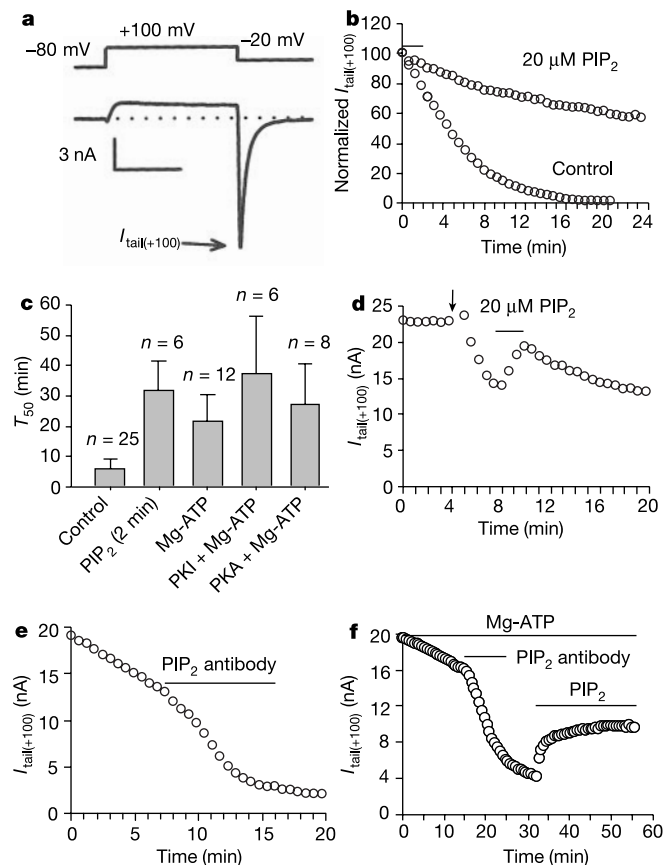


Figure 1 Stabilization of P/Q-type Ca^{2+} channel activity by PtdIns(4,5) P_2 (PIP_2). **a**, Representative current trace evoked by the indicated voltage protocol. **b**, Time course of $I_{\text{tail}(+100)}$ in control solution or with a 2-min PtdIns(4,5) P_2 treatment (unbroken line). Current is normalized to that obtained immediately after patch excision. **c**, T_{50} for decay of $I_{\text{tail}(+100)}$ in control solution, with a 2-min PtdIns(4,5) P_2 treatment (20 μM) immediately after patch excision, in 2 mM Mg-ATP, 2 mM Mg-ATP plus 5 μM PKI 5-24, or 2 mM Mg-ATP plus 8.8 units ml^{-1} PKA catalytic subunit plus 0.3 μM okadaic acid. **d**, Time course of $I_{\text{tail}(+100)}$ with a 2-min PtdIns(4,5) P_2 treatment during rundown. Arrow indicates patch excision. **e**, **f**, Acceleration of $I_{\text{tail}(+100)}$ rundown by antibodies specific for PtdIns(4,5) P_2 (28.5 $\mu\text{g ml}^{-1}$ after 1:10 dilution) in control solution (**e**) or in the presence of 2 mM Mg-ATP, with partial reactivation of rundown channels by PtdIns(4,5) P_2 (**f**). Current sign is reversed in this and following figures.

excision (Fig. 2b) and the activation curve measured 8–10 min thereafter showed only a slight shift (Fig. 2c). A 2-min application of PtdIns(4,5) P_2 caused the tail currents to bifurcate (Fig. 2d): $I_{\text{tail}(+10)}$ was inhibited immediately and rapidly to $\sim 25\%$ of its starting value, whereas $I_{\text{tail}(+100)}$ was not obviously affected. (The residual $I_{\text{tail}(+10)}$ became very steady after stopping the application of PtdIns(4,5) P_2 , supporting the notion that PtdIns(4,5) P_2 retards rundown.) This result suggests that PtdIns(4,5) P_2 profoundly alters the voltage dependence of channel activation, making channels harder to open by weak depolarizations. The activation curve measured during a 10-min application of PtdIns(4,5) P_2 showed a gradual positive shift, which reached a maximum 8–10 min during application of PtdIns(4,5) P_2 when $I_{\text{tail}(+10)}$ was inhibited completely (Fig. 2e).

The PtdIns(4,5) P_2 -induced voltage-dependent inhibition is reminiscent of the action of G proteins on N-type and P/Q-type channels^{2,16}, which has been modelled as a shift of channel gating from a ‘willing’ to a ‘reluctant’ mode on the binding of G proteins to the channel¹⁶. This model might also account for the PtdIns(4,5) P_2 inhibition. We thought that channels in the willing mode might be opened more easily by weak or moderate depolarizations than those

in the reluctant mode and that PtdIns(4,5) P_2 action might convert channels from the willing mode to the reluctant mode. According to this hypothesis, most channels would exist in the willing mode in the cell-attached configuration and immediately after patch excision (81% and 83%, respectively, $n = 37$), and a small population ($\sim 10\%$) of channels would be in the reluctant mode. Application of exogenous PtdIns(4,5) P_2 would shift most channels to the reluctant mode, reducing the fraction of willing channels from 85% to 3%, and increasing the fraction of reluctant channels from 5% to 80%.

The above results create a puzzle: if PtdIns(4,5) P_2 shifts channels to the reluctant mode, then why are most channels in intact oocytes in the willing mode? One possibility is that the endogenous PtdIns(4,5) P_2 concentration is too low to convert most channels to the reluctant mode. Another possibility is that other signalling mechanisms antagonize the inhibitory action of PtdIns(4,5) P_2 and protect the channels from PtdIns(4,5) P_2 -induced gating shift. We investigated whether PKA phosphorylation might have such a role as it regulates the interaction of PtdIns(4,5) P_2 with Kir channels¹⁷ and it produces opposite actions on Ca^{2+} channels to those induced by PtdIns(4,5) P_2 ; that is, it augments currents evoked by weak and moderate depolarizations and shifts the I - V in the negative direction^{3,18,19}.

With 2 mM Mg-ATP in the intracellular solution, PtdIns(4,5) P_2 failed to produce a substantial inhibition of $I_{\text{tail}(+10)}$ or a positive shift of the activation curve (Fig. 3a, b). This failure was observed in five of nine patches. By contrast, these PtdIns(4,5) P_2 -induced effects were observed in 25 of 25 patches without Mg-ATP. The protective action of Mg-ATP was probably due to the activation of endogenous

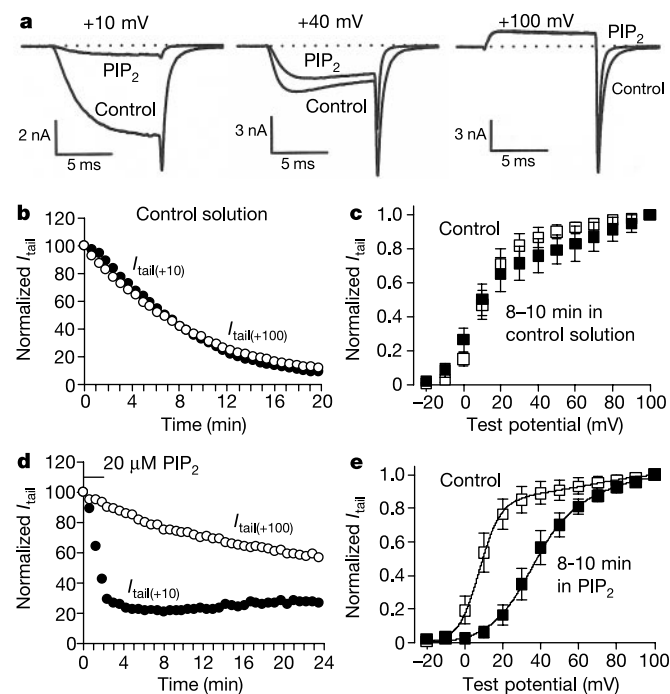


Figure 2 Voltage-dependent inhibition of P/Q-type Ca^{2+} channels by PtdIns(4,5) P_2 (PIP_2). **a**, Currents recorded immediately before and 80–100 s after application of 20 μM PtdIns(4,5) P_2 evoked by the indicated depolarization. Dotted line indicates zero current. **b**, Time course of rundown of $I_{\text{tail}(+10)}$ (filled circles) and $I_{\text{tail}(+100)}$ (open circles) in control solution. Current is normalized to that obtained immediately after patch excision. **c**, Voltage dependence of activation in control solution 1 min (open squares) and 8–10 min (filled squares) after patch excision ($n = 8$). **d**, Time course of PtdIns(4,5) P_2 action on $I_{\text{tail}(+10)}$ and $I_{\text{tail}(+100)}$. Current is normalized to that obtained before application of PtdIns(4,5) P_2 . **e**, Voltage dependence of activation before (open squares) and 8–10 min during (filled squares) application of 20 μM PtdIns(4,5) P_2 ($n = 7$). Solid lines are fitting curves (see Methods).

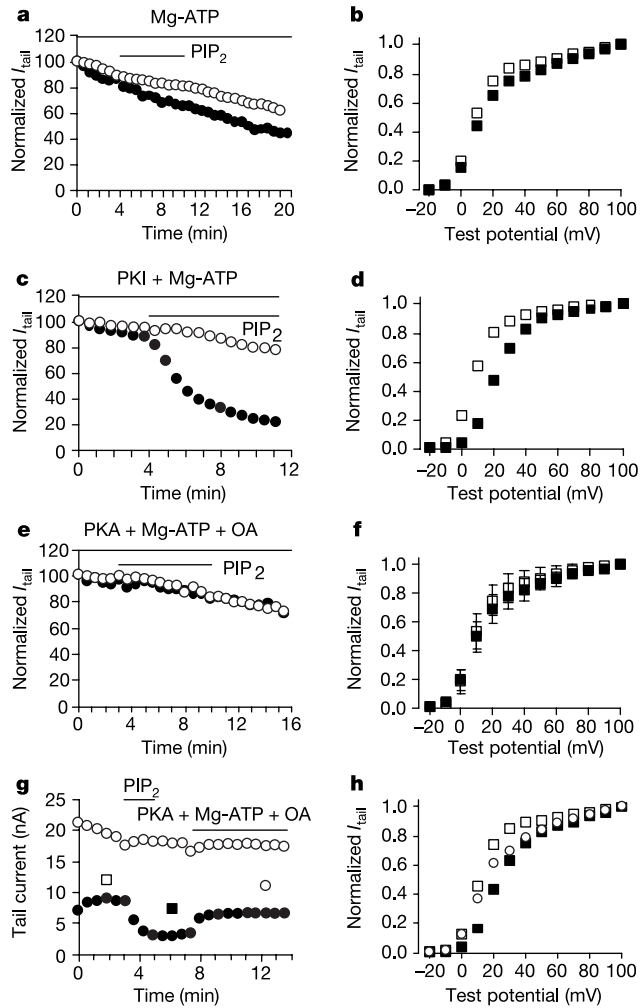


Figure 3 Crosstalk between phosphorylation by PKA and PtdIns(4,5)P₂ (PIP₂). **a, c, e**, Time course of $I_{tail(+10)}$ (filled circles) and $I_{tail(+100)}$ (open circles) in the presence of 2 mM Mg-ATP (**a**), 2 mM Mg-ATP plus 5 μ M PKI (**c**), or 2 mM Mg-ATP plus 8.8 units ml⁻¹ PKA catalytic subunit plus 0.3 μ M okadaic acid (**e**), with 20 μ M PtdIns(4,5)P₂ added during rundown. Current is normalized to that obtained immediately after patch excision. **b, d, f**, Voltage dependence of activation before (open squares) and 8–10 min after (filled squares) application of 20 μ M PtdIns(4,5)P₂. **b** and **d** are from the same patch shown in **a** and **c**, respectively, and **f** is the average of nine patches with the same experimental conditions as **e, g**. **g**, Time course of $I_{tail(+10)}$ (filled circles) and $I_{tail(+100)}$ (open circles) with PtdIns(4,5)P₂ treatment, followed by 2 mM Mg-ATP plus 8.8 units ml⁻¹ PKA catalytic subunit plus 0.3 μ M okadaic acid. **h**, Voltage dependence of activation obtained at the times indicated by the symbols described in **g**.

PKA in the patch because the PtdIns(4,5)P₂ effects were restored when PKI 5-24 (1–5 μ M) or H-89 (2 μ M), both of which are potent inhibitors of PKA, was added with Mg-ATP (6/7 patches for PKI 5-24 and 5/7 patches for H-89; Fig. 3c, d). When phosphorylation by PKA was strongly promoted by adding the catalytic subunit of PKA and okadaic acid together with Mg-ATP, the variability seen with Mg-ATP alone was eliminated and, in nine of nine patches, PtdIns(4,5)P₂ no longer inhibited $I_{tail(+10)}$ (Fig. 3e) or shifted the activation curve (Fig. 3f). In addition, after $I_{tail(+10)}$ was reduced by a 2-min pulse of PtdIns(4,5)P₂, subsequent application of a mixture that promoted PKA phosphorylation could quickly (albeit partially) recover the current (Fig. 3g) and shift the activation curve back towards the control curve (Fig. 3h), suggesting that phosphorylation by PKA can revert channels from the reluctant to the willing mode. By comparison, no such fast recovery was observed after washing out PtdIns(4,5)P₂ with the control solution (Fig. 2d).

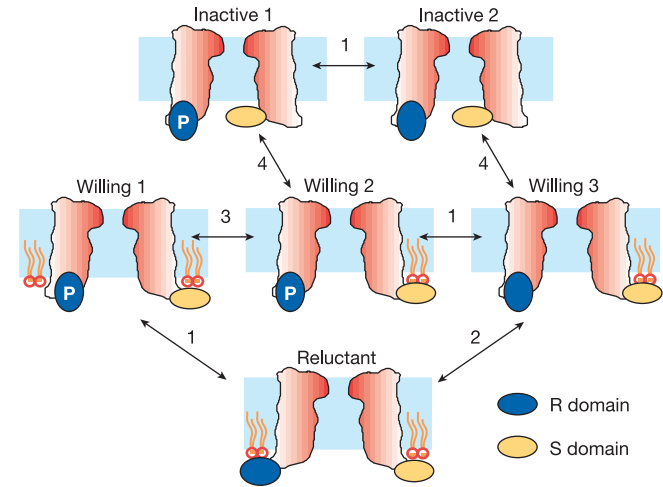


Figure 4 Model of modulation of P/Q-type Ca²⁺ channels by PtdIns(4,5)P₂ and PKA. The channel contains two distinct PtdIns(4,5)P₂-binding domains: the high-affinity S (for stabilization) domain and the low-affinity R (for reluctant and regulatory) domain. The latter can be phosphorylated by PKA, which dislodges PtdIns(4,5)P₂ from this domain. Channels without PtdIns(4,5)P₂ bound to the S domain are inactive, whereas those with and without PtdIns(4,5)P₂ on the R domain are in the reluctant and willing mode, respectively. Transitions between the various modulated states represent phosphorylation or dephosphorylation of the R domain (transition 1); binding or unbinding of PtdIns(4,5)P₂ to or from the R domain (transition 2); removal or addition of PtdIns(4,5)P₂ from or to the membrane (transition 3); and binding and unbinding of PtdIns(4,5)P₂ to or from the S domain (transition 4).

These results indicate that phosphorylation by PKA not only prevents but also reverses PtdIns(4,5)P₂-induced inhibition. We also attempted to increase endogenous phosphorylation by PKA by treating intact oocytes with forskolin or 8-bromo cyclic AMP; however, these treatments failed to produce any clear and consistent effect on P/Q-type channel currents.

The sites of PtdIns(4,5)P₂ binding and PKA phosphorylation remain to be determined. Because the Ca_v2.1 subunit contains several consensus sites for PKA phosphorylation²⁰ and PtdIns(4,5)P₂ binds directly to Kir channels¹⁰, we thought that the P/Q-type channel itself might be the target. We therefore propose a model (Fig. 4) in which P/Q-type channels possess two distinct PtdIns(4,5)P₂ binding sites: the S domain binds PtdIns(4,5)P₂ to stabilize channel activity, and the R domain binds PtdIns(4,5)P₂ to shift channels to the reluctant mode. The S domain has a higher affinity for PtdIns(4,5)P₂ than has the R domain. Finally, phosphorylation of the R domain by PKA markedly lowers its affinity for PtdIns(4,5)P₂ through electrostatic repulsion and/or allosteric conformational changes and converts channels to the willing mode.

This model can satisfactorily explain our experimental results. In intact oocytes, the concentration of endogenous PtdIns(4,5)P₂ is sufficiently high to maintain the activity of most channels by binding to the S domain. Owing to PKA phosphorylation and/or lower affinity, most channels are devoid of PtdIns(4,5)P₂ in the R domain and are thus in one of three interconvertible willing states, which we assume are biophysically indistinguishable. A very few channels that are not phosphorylated by PKA and bound to PtdIns(4,5)P₂ in the R domain are in the reluctant mode. After patch excision, the concentration of PtdIns(4,5)P₂ gradually decreases (presumably owing to dephosphorylation by lipid phosphatases), resulting in the unbinding of PtdIns(4,5)P₂ from the S domain and causing the channels to enter an inactive state (that is, rundown). Meanwhile, most channels are rapidly dephosphorylated and become susceptible to PtdIns(4,5)P₂ binding to the R domain. Thus, the application of exogenous PtdIns(4,5)P₂ on the

one hand restores PtdIns(4,5)P₂ binding to the S domain, thereby increasing the number of functional channels and stabilizing channel activity, and on the other hand converts channels to the reluctant mode. Phosphorylation by PKA interferes with PtdIns(4,5)P₂ binding to the R domain, not only preventing this conversion but also shifting reluctant channels back to the willing mode.

We next studied the effect of receptor-mediated hydrolysis of PtdIns(4,5)P₂ on whole-oocyte P/Q-type currents. To avoid complications from G-protein-induced inhibition, we examined the nerve growth factor (NGF)-activated TrkA receptor, which stimulates PtdIns(4,5)P₂ hydrolysis by directly activating phospholipase C-γ (PLC-γ)²¹. According to our model (Fig. 4), depletion of PtdIns(4,5)P₂ in intact oocytes should have two sequential functional effects: first, it should shift the small fraction (~10%) of reluctant channels to the willing mode; and second, it should induce channel downregulation. We found that NGF produces a biphasic effect on current elicited by depolarization to +10 mV (*I*_{peak(+10)}): the current increased transiently and then decreased even after washout of the agonist (Fig. 5a), probably owing to prolonged activation of TrkA receptors and/or downstream signalling pathways²². The average increase and decrease were 9 ± 6% and 34 ± 19% (*n* = 31), respectively. The *I*-*V* curve measured during the enhancement showed a slight negative shift, consistent with conversion of reluctant channels to the willing mode, and the curve measured during the inhibition was essentially a scale down, as expected from channel rundown to the inactive state (Supplementary Information).

Activation of TrkA receptors leads to stimulation of the mitogen-activated-protein-kinase (MAPK) pathway and PLC-γ²¹, which catalyses the hydrolysis of PtdIns(4,5)P₂ into diacylglycerol (DAG) and inositol-1,4,5-triphosphate (InsP₃), two second-messengers that activate protein kinase C (PKC) and release Ca²⁺ from intracellular stores, respectively. Much evidence indicates that the NGF-induced effects resulted directly from TrkA receptor-mediated breakdown of PtdIns(4,5)P₂ rather than downstream signalling molecules and pathways. First, activation of the Tyr499Phe mutant of TrkA, which is uncoupled from the MAPK pathway^{13,21}, produced

similar effects (8.4 ± 3.8% increase followed by 15.4 ± 10% inhibition, *n* = 18) to those of wild-type receptors. But activation of the Tyr794Phe mutant TrkA, which is unable to stimulate PLC-γ^{13,21}, produced neither enhancement nor inhibition (Fig. 5b), indicating that hydrolysis of PtdIns(4,5)P₂ is essential for both actions. Second, preincubation of oocytes with thapsigargin, which depletes intracellular Ca²⁺ stores, abolished NGF-induced increase in intracellular concentrations of Ca²⁺ but did not affect the NGF-induced regulation of P/Q-type channels (9.0 ± 6.4% increase, 42 ± 16.4% inhibition, *n* = 10, Fig. 5c), indicating that InsP₃-induced release of Ca²⁺ has no role. Third, activation of PKC by a phorbol ester, phorbol-12-myristate-13-acetate (PMA) (10–500 nM), produced a similar biphasic effect on P/Q-type channels as did NGF (8 ± 4% increase, 30 ± 18% inhibition, *n* = 14). But, whereas PMA-induced regulation was completely blocked by the PKC inhibitor bisindolylmaleimide I in 17 of 22 oocytes, the NGF-induced effects remained unchanged in 12 of 14 oocytes (8.0 ± 4.4% increase, 31 ± 16% inhibition, *n* = 12, Fig. 5d). These results indicate although PKC activation regulates P/Q-type channels, it is not required for the NGF action. Last, application of InsP₃ (100 μM) or DAG (20 μM) to the intracellular side in inside-out patches had no effect on *I*_{tail(+10)} or *I*_{tail(+100)}, indicating that these second messengers do not mediate the effects of NGF (Supplementary Information).

We further investigated whether PtdIns(4,5)P₂ regulates the activity of VGCCs in native cells. In bullfrog sympathetic neurons, the neuropeptide chicken type II luteinizing hormone-releasing hormone (LHRH) induces both voltage-dependent and voltage-independent inhibition of N-type Ca²⁺ channels²³. Because stimulation of LHRH receptors activates PLC²⁴, we tested the hypothesis that the latter effect may be the result of PtdIns(4,5)P₂ breakdown. With a physiological concentration (~213 nM) of free Ca²⁺ in the pipette solution, LHRH markedly inhibited the tail current after pulses to +60 mV (*I*_{tail(+60)}) (Fig. 5e). There was usually no or only partial recovery after washout of LHRH. This inhibition was largely voltage independent (Fig. 5g). Notably, the voltage-independent component was significantly greater than that obtained with low concentrations (~10 nM) of free Ca²⁺ (ref. 23), consistent with a

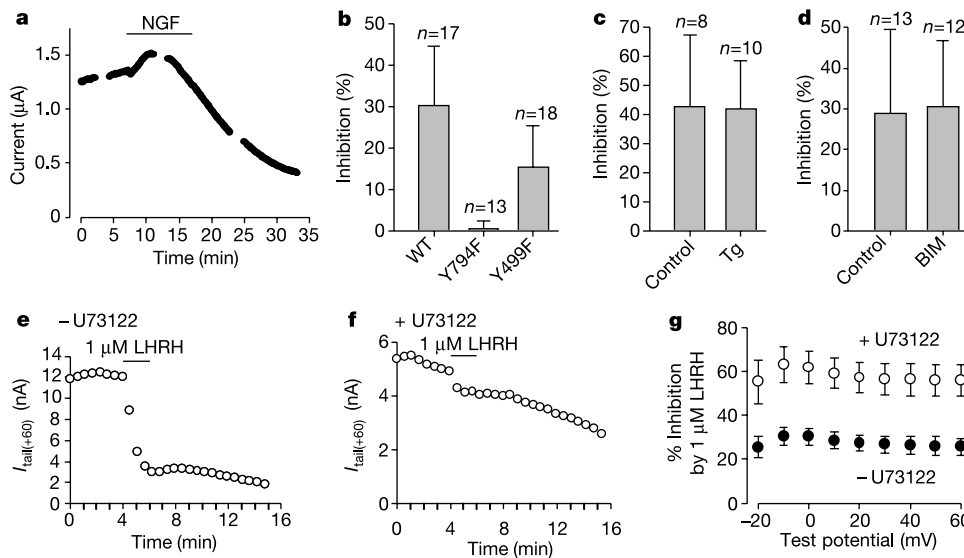


Figure 5 Regulation of P/Q- and N-type Ca²⁺ channels through receptor-mediated hydrolysis of PtdIns(4,5)P₂. **a–d**, P/Q-type channels in oocytes. **a**, Biphasic effect of NGF (100 ng ml⁻¹) on the whole-oocyte *I*_{peak(+10)} in an oocyte expressing TrkA receptors. *I*-*V* curves were measured during the gaps. **b–d**, Comparison of NGF-induced inhibition of *I*_{peak(+10)} in oocytes under various experimental conditions: expression of either wild-type or mutant TrkA receptors (**b**); with or without overnight thapsigargin (Tg, 100 nM)

treatment (**c**); and with or without overnight bisindolylmaleimide I (BIM, 10 μM) preincubation (**d**). **e–g**, N-type channels in bullfrog sympathetic neurons. **e, f**, Inhibition of *I*_{tail(+60)} by LHRH in a neuron without (**e**) and with (**f**) U73122 preincubation (5 μM for 10 min). **g**, Comparison of LHRH-induced inhibition of the tail current after depolarization to the indicated voltages in neurons without (*n* = 8) and with (*n* = 6) U73122 pretreatment. Error bars represent s.e.m.

role for PLC, which requires Ca^{2+} for maximal activity²⁵. Most notably, the LHRH-induced inhibition was greatly attenuated in neurons pretreated with a membrane-permeable PLC inhibitor U73122 (Fig. 5f, g); however, it was not altered by pretreating the neurons with a PKC blocker staurosporin (0.5–1 μ M for 30 min); LHRH reduced $I_{tail(+60)}$ by $62 \pm 11\%$ ($n = 7$) and $62 \pm 7\%$ ($n = 4$) in untreated and treated neurons, respectively. In addition, dialysing the cells with 100 μ M InsP₃ neither inhibited the current nor occluded LHRH-induced inhibition ($50 \pm 7\%$, $n = 4$). These results suggest that the LHRH-induced inhibition is most probably a direct consequence of a decrease in the membrane quantity of PtdIns(4,5)P₂ rather than being mediated by PKC, InsP₃ or Ca^{2+} . In our model (Fig. 4), this inhibition corresponds to the conversion of active channels (predominantly in the willing mode) to inactive channels owing to loss of PtdIns(4,5)P₂ from the stabilization domain.

Our study shows that PtdIns(4,5)P₂ has two distinct and opposing actions on VGCCs: stabilization of channel activity and voltage-dependent inhibition. A further twist is that the inhibitory action can be prevented and reversed by phosphorylation by PKA. Thus, the precise modulatory action of PtdIns(4,5)P₂ on VGCCs depends not only on the dynamic concentration of membrane PtdIns(4,5)P₂, which is determined by the activities of phospholipases as well as lipid kinases and phosphatases, but also on the concentration and state of other signalling pathways. As PtdIns(4,5)P₂ and its regulating enzymes are present at synapses^{26–28}, and PtdIns(4,5)P₂ is thought to be important in exocytosis and endocytosis^{27,28}, regulation of VGCCs by PtdIns(4,5)P₂ could have profound consequences on synaptic transmission and plasticity.

Note added in proof: While this paper was being revised, a paper on modulation of M-current channels by PtdIns(4,5)P₂ appeared: Suh, B.-C. & Hille, B. Recovery from muscarinic modulation of M current channels requires phosphatidylinositol 4,5-bisphosphate synthesis. *Neuron* **35**, 507–520 (2002). □

Methods

Oocyte expression and neuron isolation

Rabbit brain Ca_v2.1, rat brain β_4 , rabbit skeletal muscle $\alpha_2\delta$, rat TrkA and its mutants, and rat p75 were subcloned into variants of pGEMHE or pUCHE. We synthesized cRNAs *in vitro* and injected them in various combinations into *Xenopus* oocytes, which were obtained and maintained as described²⁹.

Sympathetic ganglia were isolated from mature bullfrogs (*Rana catesbeiana*) and single neurons were isolated as described³⁰. The dissociated cells were kept in 73% L15 medium (4°C) and used within 48 h.

Electrophysiology

For two-electrode voltage-clamp studies, the electrodes were filled with 3 M KCl and had resistances of ~0.5–1 M Ω . The bath solution contained (in mM) 10 BaCl₂, 5 KCl, 60 tetraethylammonium ion (TEA)-OH, 20 NaOH and 5 HEPES (pH 7.4 with HCl). Currents were evoked every 6 s by 40-ms depolarizations to various levels from a holding potential of –80 mV. For macropatch recordings from oocytes, the pipettes had a diameter of 15–30 μ m and were filled with a solution containing (in mM) 45 BaCl₂, 80 KCl and 10 HEPES (pH 7.3 with KOH). The control bath solution contained (in mM) 125 KCl, 4 NaCl, 10 HEPES and 10 EGTA (pH 7.3 with KOH). Macroscopic currents were evoked from a holding potential of –80 mV every 3 s by 10-ms depolarizations ranging from –20 mV to +100 mV in 10-mV increments, followed by a 15-ms repolarization to –20 mV. For whole-cell recordings from sympathetic neurons, the pipettes were fire-polished and had resistances of ~2–3 M Ω when filled with a solution containing (in mM) 120 CsCl, 10 HEPES, 8 EGTA, 2 MgCl₂, 5 CaCl₂, 2 Na₂-ATP and 0.5 Na-GTP (pH 7.3 with CsOH). The series resistance was compensated by 70–90%. The control bath solution contained (in mM) 2 BaCl₂, 145 TEA-Cl, 10 glucose and 10 HEPES (pH 7.3 with TEA-OH), with 2.5 μ M nimodipine to block L-type channels. Currents were evoked from a holding potential of –80 mV every 3 s by 15-ms depolarizations from –50 mV to +60 mV in 10-mV increments, followed by a 15-ms repolarization to –50 mV. Currents were filtered at 2 kHz, digitized at 10–50 kHz and analysed with pClamp8 (Axon Instruments). We carried out experiments at 20–22°C.

We used the following reagents: purified brain PtdIns(4,5)P₂ (Avanti Polar Lipids), which was sonicated for about 15 min before application; the catalytic subunit of PKA, okadaic acid, PKI 5-24, PMA, diacylglycerol, U73122, bisindolylmaleimide I, staurosporin and H-89 (Calbiochem); antibodies against PtdIns(4,5)P₂ and PtdInsP (Assay Designs); Mg-ATP, thapsigargin, InsP₃, nimodipine and trypsin (Sigma); NGF and disperse II (Boehringer Mannheim); collagenase type I (Worthington Biochemical); and chicken type II LHRH (Peninsula Laboratories). Stock solutions of water-insoluble reagents were made

in dimethyl sulphoxide, stored at –20°C and diluted to appropriate final concentrations before use.

Data analysis

The voltage-dependence of channel activation was fitted with the sum of three Boltzmann functions of the form $f_1 \cdot 1 / (1 + \exp[-(V - V_1) / k_1]) + f_2 \cdot 1 / (1 + \exp[-(V - V_2) / k_2]) + f_3 \cdot 1 / (1 + \exp[-(V - V_3) / k_3])$, where f_x , V_x and k_x are, respectively, the fraction, midpoint of activation and slope factor of the three components, with the constraint of $f_1 + f_2 + f_3 = 1$. The first two functions describe the willing and reluctant channels, respectively, with parameters $V_1 = 7.7$ mV, $k_1 = 5.5$ mV, $V_2 = 35$ mV and $k_2 = 10$ mV, which were chosen by fitting the activation curves, obtained either in cell-attached recordings or 8–10 min after application of 20 μ M PtdIns(4,5)P₂, with the sum of two Boltzmann components. The third function has no theoretical meaning but is required to correct for voltage-dependent inactivation, which is most pronounced for inward currents evoked by depolarizations between +30 and +70 mV. V_3 and k_3 are 73 mV and 13.7 mV, respectively, on the basis of fitting the activation curve from patches that showed relatively strong inactivation. Thus, in the final fitting process, the only variables were the fractions of the three components.

T_{50} was defined as the time for current to decay to 50% of its starting value. In cases in which the recording was lost before T_{50} was reached, the decay phase of the current was fitted with either a single or double exponential function and T_{50} was extrapolated on the basis of the fitting. These patches were held for more than 15 min after patch excision and thus T_{50} was more than 15 min. About 50–70% of the patches under each condition (except the control) in Fig. 1c were analysed by this method. To verify the validity of such analysis, we intentionally truncated the data to 15 min from two 30-min recordings and found that the extrapolated T_{50} was nearly identical to the measured value. In experiments to study the effect of NGF on P/Q-type channels, NGF (100 ng ml⁻¹) was applied for 9 min. The effect was quantified according to the equation $I_x / I_{con} = 100 \cdot [(I_{con} - I_x) / I_{con}]$, where I_{con} is the current immediately before NGF application and I_x is the maximum current during NGF application (enhancement) or the current obtained 9 min after washout of NGF (inhibition).

Unless indicated otherwise, data are presented as the mean \pm s.d., with the number of observations in parentheses.

Received 8 July; accepted 20 August 2002; doi:10.1038/nature01118.

- Hille, B. *Ion Channels of Excitable Membranes* (Sinauer, Sunderland, 2001).
- Catterall, W. A. Structure and regulation of voltage-gated Ca²⁺ channels. *Annu. Rev. Cell Dev. Biol.* **16**, 521–555 (2000).
- McDonald, T. F., Pelzer, S., Trautwein, W. & Pelzer, D. J. Regulation and modulation of calcium channels in cardiac, skeletal, and smooth muscle cells. *Physiol. Rev.* **74**, 365–507 (1994).
- Chad, J. E. & Eckert, R. An enzymatic mechanism for calcium current inactivation in dialysed *Helix* neurons. *J. Physiol. (Lond.)* **378**, 31–51 (1986).
- Armstrong, D. & Eckert, R. Voltage-activated calcium channels that must be phosphorylated to respond to membrane depolarization. *Proc. Natl Acad. Sci. USA* **84**, 2518–2522 (1987).
- Hao, L. Y., Kameyama, A. & Kameyama, M. A cytoplasmic factor, calpastatin and ATP together reverse run-down of Ca²⁺ channel activity in guinea-pig heart. *J. Physiol. (Lond.)* **514**, 687–699 (1999).
- Hilgemann, D. W. & Ball, R. Regulation of cardiac Na⁺, Ca²⁺ exchange and K_{ATP} potassium channels by PIP₂. *Science* **273**, 956–959 (1996).
- Hilgemann, D. W. Cytoplasmic ATP-dependent regulation of ion transporters and channels: mechanisms and messengers. *Annu. Rev. Physiol.* **59**, 193–220 (1997).
- Hilgemann, D. W., Feng, S. & Nasuhoglu, C. The complex and intriguing lives of PIP₂ with ion channels and transporters. *Science STKE* [online] (http://stke.sciencemag.org/cgi/content/full/OC_sigtrans;2001/111/re19) (2001).
- Huang, C.-L., Feng, S. & Hilgemann, D. W. Direct activation of inward rectifier potassium channels by PIP₂ and its stabilization by G_{βγ}. *Nature* **391**, 803–806 (1997).
- Womack, K. B. *et al.* Do phosphatidylinositides modulate vertebrate phototransduction? *J. Neurosci.* **20**, 2792–2799 (2000).
- Kobrinshi, E., Mirshahi, T., Zhang, H., Jin, T. & Logothetis, D. E. Receptor-mediated hydrolysis of plasma membrane messenger PIP₂ leads to K⁺-current desensitization. *Nature Cell Biol.* **2**, 507–514 (2000).
- Chuang, H.-h. *et al.* Bradykinin and nerve growth factor release the capsaicin receptor from PtdIns(4,5)P₂-mediated inhibition. *Nature* **411**, 957–962 (2001).
- Runnels, L. W., Yue, L. & Clapham, D. E. The TRPM7 channel is inactivated by PIP₂ hydrolysis. *Nature Cell Biol.* **4**, 329–336 (2002).
- Fukami, K. *et al.* Antibody to phosphatidylinositol 4,5-bisphosphate inhibits oncogene-induced mitogenesis. *Proc. Natl Acad. Sci. USA* **85**, 9057–9061 (1988).
- Bean, B. P. Neurotransmitter inhibition of neuronal calcium currents by changes in channel voltage dependence. *Nature* **340**, 153–156 (1989).
- Liou, H.-H., Zhou, S.-S. & Huang, C.-L. Regulation of ROMK1 channel by protein kinase A via a phosphatidylinositol 4,5-bisphosphate-dependent mechanism. *Proc. Natl Acad. Sci. USA* **96**, 5820–5825 (1999).
- Bean, B. P. *Ion Channels in the Cardiovascular System; Function and Dysfunction* (eds Spooner, P. M., Brown, A. M., Catterall, W. A., Kaczorowski, G. J. & Strauss, H. C.) 237–252 (Futura, New York, 1994).
- Bean, B. P., Nowycky, M. C. & Tsien, R. W. β -Adrenergic modulation of calcium channels in frog ventricular heart cells. *Nature* **307**, 371–375 (1984).
- Mori, Y. *et al.* Primary structure and functional expression from complementary DNA of a brain calcium channel. *Nature* **350**, 398–402 (1991).
- Stephens, R. *et al.* Trk receptors use redundant signal transduction pathways involving SHC and PLC- γ 1 to mediate NGF responses. *Neuron* **12**, 691–705 (1994).
- Choi, D.-Y., Toledo-Aral, J. J., Segal, R. & Halegoua, S. Sustained signaling by phospholipase C- γ mediates nerve growth factor-triggered gene expression. *Mol. Cell Biol.* **21**, 2695–2705 (2001).
- Boland, L. M. & Bean, B. P. Modulation of N-type calcium channels in bullfrog sympathetic neurons by luteinizing hormone-releasing hormone: kinetics and voltage dependence. *J. Neurosci.* **12**, 516–533 (1993).

24. McArdele, C. A., Franklin, J., Green, L. & Hislop, J. N. Signaling, cycling and desensitization of gonadotrophin-releasing hormone receptors. *J. Endocrinol.* **173**, 1–11 (2002).
25. Rhee, S. G. Regulation of phosphoinositides-specific phospholipase C. *Annu. Rev. Biochem.* **70**, 281–312 (2001).
26. McPherson, P. S. *et al.* A presynaptic inositol-5-phosphatase. *Nature* **379**, 353–357 (1996).
27. Wenk, M. R. *et al.* PIP kinase $\text{I}\gamma$ is the major PI(4,5) P_2 synthesizing enzyme at the synapse. *Neuron* **32**, 79–88 (2001).
28. Cremona, O. & De Camilli, P. Phosphoinositides in membrane traffic at the synapse. *J. Cell Sci.* **114**, 1041–1052 (2001).
29. Lu, T., Nguyen, B., Zhang, X.-M. & Yang, J. Architecture of a K^+ channel inner pore revealed by stoichiometric covalent modification. *Neuron* **22**, 571–580 (1999).
30. Yang, J. & Tsien, R. W. Enhancement of N- and L-type calcium channel currents by protein kinase C in frog sympathetic neurons. *Neuron* **10**, 127–136 (1993).

Supplementary Information accompanies the paper on Nature's website
(<http://www.nature.com/nature>).

Acknowledgements We thank S. Siegelbaum for comments on the manuscript; Y. Mori for $\text{Ca}_v2.1$ cDNA; E. Perez-Reyes for $\beta 4$ cDNA; T. Tanabe for $\alpha 2\delta$ cDNA; D. J. Julius for p75 and TrkA (wild-type and mutant) cDNAs. This work was supported by a grant to J.Y. from the National Heart, Lung, and Blood Institute. J.Y. is a recipient of the McKnight Scholar Award and the Scholar Research Programme of the EJLB Foundation.

Competing interests statement The authors declare that they have no competing financial interests.

Correspondence and requests for materials should be addressed to J.Y.
(e-mail: jy160@columbia.edu).

Thiamine derivatives bind messenger RNAs directly to regulate bacterial gene expression

Wade Winkler*, Ali Nahvi† & Ronald R. Breaker*

* Department of Molecular, Cellular and Developmental Biology, and

† Department of Molecular Biophysics and Biochemistry, Yale University, PO Box 208103, New Haven, Connecticut 06520-8103, USA

Although proteins fulfil most of the requirements that biology has for structural and functional components such as enzymes and receptors, RNA can also serve in these capacities. For example, RNA has sufficient structural plasticity to form ribozyme^{1,2} and receptor^{3,4} elements that exhibit considerable enzymatic power and binding specificity. Moreover, these activities can be combined to create allosteric ribozymes^{5,6} that are modulated by effector molecules. It has also been proposed^{7–12} that certain messenger RNAs might use allosteric mechanisms to mediate regulatory responses depending on specific metabolites. We report here that mRNAs encoding enzymes involved in thiamine (vitamin B₁) biosynthesis in *Escherichia coli* can bind thiamine or its pyrophosphate derivative without the need for protein cofactors. The mRNA–effector complex adopts a distinct structure that sequesters the ribosome-binding site and leads to a reduction in gene expression. This metabolite-sensing regulatory system provides an example of a ‘riboswitch’ whose evolutionary origin might pre-date the emergence of proteins.

A thiamine pyrophosphate (TPP)-dependent sensor/regulatory protein has been proposed to participate in the control of thiamine biosynthetic genes¹³, but thus far no such protein factor has been shown to exist. Recently, we established that the mRNA leader sequence of the *btuB* gene of *E. coli* can bind coenzyme B₁₂ selectively, and that this binding event brings about a structural change in the RNA that is important for genetic control¹⁴. In the current study, we set out to determine whether mRNAs that encode thiamine biosynthetic proteins might also use a riboswitch that is

located in their untranslated leader sequence. We prepared β -galactosidase translational fusion constructs that encompass the 5'-untranslated regions of *thiM* and *thiC* mRNAs of *E. coli*, each of which includes a previously identified ‘*thi* box’ domain whose sequence and potential secondary structure are conserved in several species of bacteria and archaea¹¹. The *thiM* and *thiC* translational fusion constructs exhibit thiamine-dependent suppression of β -galactosidase activity of 18- and 110-fold, respectively, when host cells are grown in a minimal medium. A transcriptional fusion containing the *thiM* leader is not subject to suppression by thiamine, but a similar fusion with *thiC* leader yields a 16-fold modulation with thiamine, suggesting that a significant portion of genetic control observed with *thiC* occurs at the level of transcription.

These constructs were subsequently used to prepare DNA templates by polymerase chain reaction (PCR) for *in vitro* transcription of RNA fragments. The resulting RNAs were subjected to a structure-probing process^{14–16} to reveal whether the RNAs undergo structure modulation upon binding of ligands. Internucleotide linkages in unstructured regions are more likely to undergo spontaneous cleavage compared to linkages that reside in highly structured regions of an RNA¹⁵. The 165-nucleotide *thiM* RNA fragment (165 *thiM*) has a distinct pattern of cleavage products that is generated when the RNA is incubated for an extended period in the absence of TPP (Fig. 1a). Upon addition of 100 μM TPP, 165 *thiM* undergoes substantial structural alteration, with many internucleotide linkages in the region spanning positions 39–80 exhibiting a reduction in spontaneous cleavage. This indicates that TPP binds to the RNA and stabilizes a defined structure within this region, resulting in a lower rate of fragmentation.

The fragmentation patterns are largely congruent with potential stem and bulge structures that are identified by a secondary-structure prediction algorithm^{17,18}. Most linkages that experience a ligand-induced reduction of cleavage are encompassed by the *thi* box and nucleotides that reside immediately 5' relative to this domain (Fig. 1b). Other linkages that undergo cleavage, but that are not modulated by TPP, are predicted to reside in bulges or in the loops of hairpins. Predicted base-paired structures labelled P2–P7 include linkages that exhibit the lowest levels of spontaneous cleavage, implying that they remain structured in both the presence and absence of TPP. Nucleotides 126–130 encompass the only region apart from those described above that becomes more structured upon TPP addition. These nucleotides correspond to the Shine–Dalgarno (SD) sequence, which is required to be unpaired for efficient translation of mRNAs in prokaryotes. These findings are consistent with a genetic control mechanism in which the *thiM* RNA binds to TPP and forms a complex such that the ribosome cannot gain access to the SD sequence.

Similarly, structure probing was used to examine the mRNA leader for *thiC*. The 240 *thiC* RNA also exhibits extensive modulation of its pattern of spontaneous cleavage, and again the majority of the changing pattern is located in the *thi* box and in the region located immediately upstream of this domain (Fig. 1c). These regions of highest structure modulation in *thiM* and *thiC* can be folded into similar secondary structures (Fig. 1d), and carry several common sequence elements within and adjacent to the *thi* box domain. Therefore, we propose that the structures of *thiM* and *thiC* spanning stems P1–P5 comprise TPP-binding motifs that are analogous to aptamers, which are engineered ligand-binding RNAs^{3,4,19}. Nucleotides residing 3' relative to this natural TPP aptamer are probably involved in converting the metabolite binding event into a genetic response (see below).

The sensitivity of metabolite detection by these mRNAs was assessed by establishing apparent dissociation constant (apparent K_D) values for TPP, thiamine, and thiamine monophosphate (TP). Values were generated by monitoring the extent of spontaneous cleavage at several ligand-sensitive sites within the RNA over a range